

Kinetic Full Wave Analysis of Electron Cyclotron Wave Mode Conversion in Tokamak Plasmas^{*})

Shabbir A. KHAN^{1,2)}, Atsushi FUKUYAMA¹⁾, Hiroe IGAMI³⁾ and Hiroshi IDEI⁴⁾

¹⁾Department of Nuclear Engineering, Kyoto University, Kyoto 615-8540, Japan

²⁾National Center for Physics, QAU Campus, Islamabad 45320, Pakistan

³⁾National Institute for Fusion Science, Toki 509-5292, Japan

⁴⁾Research Institute for Applied Mathematics, Kyushu University, Kasuga, Fukuoka 816-8580, Japan

(Received 2 December 2015 / Accepted 18 March 2016)

By employing the integral formulation of dielectric tensor, we have introduced the kinetic full wave analysis of ordinary-extraordinary-Bernstein (O-X-B) mode conversion in tokamak plasma in one dimension on the basis of TASK/W1 code using the finite element method. The boundary value problem of Maxwell's equation is solved and the finite Larmor radius effects are represented by integral formulation. The O-X-B mode conversion and the absorption near the cyclotron harmonic resonance are successfully described.

© 2016 The Japan Society of Plasma Science and Nuclear Fusion Research

Keywords: dielectric tensor, full wave analysis, O-X-B mode conversion, Larmor radius, Bernstein wave

DOI: 10.1585/pfr.11.2403070

1. Introduction

The electromagnetic waves in the electron cyclotron (EC) range of frequencies have been successfully applied to the electron cyclotron heating (ECH) and current drive (ECCD) in fusion devices. EC waves are extremely useful due to the fact that they can be launched far from the plasma and have features of highly localized and controllable heating capabilities.

The remarkable advantages of ECH and ECCD in high density plasma core have led great interest in theoretical and experimental investigations of EC waves in past decades [1–5]. Electromagnetic (EM) plasma waves such as ordinary (O) or extraordinary (X) waves suffer the wave cutoffs in high-density regions. This is particularly noticed in spherical tokamaks (STs) operated in high- β regimes generally, in which the usual O- and X-modes are cut off. In this case, electron Bernstein waves (EBWs) seem to be the option which provide the penetration to the high-density region.

Bernstein waves need to be excited externally through mode conversion of injected EM waves owing to high temperature in fusion plasmas. Well known schemes of mode conversion include high field side launch of wave, direct eXtraordinary Bernstein (X-B) mode conversion and Ordinary-eXtraordinary-Bernstein (O-X-B) mode conversion. Among them, the O-X-B mode conversion technique [6] is the most promising of ECH/ECCD in over-dense plasmas both in tokamaks and stellarators [7–9]. At specific launching angle, an O-mode wave converts to X-mode at a cutoff frequency. After this conversion, the wave

propagate backwards to the plasma edge till it encounters the upper hybrid resonance (UHR) layer. Since electron Bernstein wave is a quasi-electrostatic mode required to be excited in UHR layer, hence, a second mode conversion takes place from X-mode into an electron Bernstein wave. Electron Bernstein wave heating and current drive is an attractive candidate for sustaining a steady state ST plasma [5, 10, 11]. Accurate understanding of mode conversion processes in fusion devices is important both for the interpretation of diagnostic data and quantitative analysis of ECH and/or ECCD.

Usual analysis of propagation and absorption of EC waves employs ray tracing method based on geometrical optics for waves with short wavelength [12, 13]. In a plasma with high density or low magnetic field, however, the presence of cutoff layer may prevent the waves from penetrating into the central part from the low field side. Therefore full wave analysis in which Maxwell's equation is solved as a boundary-value problem is required for self-consistent description of the RF waves. In a hot plasma, however, we have to include kinetic effects, especially finite Larmor radius (FLR) effects, in the full wave analysis. Several schemes have been developed to describe the FLR effects and implemented in the numerical codes. One is to expand the FLR effects in the powers of $k_{\perp}\rho$ where k_{\perp} is the wave number perpendicular to the magnetic field and ρ is the Larmor radius. This analysis is limited to $|k_{\perp}\rho| < 1$ and is usually limited up to the second order, e.g. the TORIC code [14]. Therefore this scheme is not applicable to the situation where $k_{\perp}\rho \gtrsim 1$. The second scheme is to apply the Fourier analysis to inhomogeneous plasmas and sum up all the Fourier components of the dielectric ten-

author's e-mail: shabbir.khan.36m@st.kyoto-u.ac.jp

^{*}) This article is based on the presentation at the 25th International Toki Conference (ITC25).

sor. This scheme has been successfully applied to the ion cyclotron heating using the AORSA code [15]. Since all Fourier components are coupled with each other, a large-size matrix equation with a dense coefficient matrix has to be solved. Therefore it is prohibitive to apply this scheme to EC waves with short wave-length in tokamak plasmas. We have developed a third scheme to describe the dielectric tensor as an integral operator and solve the integro-differential Maxwell's equation [16] by the finite element method (FEM). Preliminary analysis of this scheme was applied to the IC waves in the presence of energetic particle scheme [17]. Merit of the integro-differential approach is that, since the wave number is not used in this approach, it is applicable to the cases where $k_{\perp}\rho > 1$ and that the interaction with wave electric field is spatially localized within gyro radius of particles, and therefore the coefficient matrix is sparse and less computational resource is required. In the present article, the full wave analysis of the electron Bernstein waves in tokamak plasmas is reported for the first time. Though the analysis is one-dimensional and small-size plasma at present, it seems feasible to extend to two-dimensional and large-size plasma.

In this paper, we introduce one-dimensional kinetic full wave analysis using the integro-differential approach in section 2, apply it to the O-X-B mode conversion in tokamak configuration in section 3, and summary and discussion are given in section 4.

2. Theoretical Formulation of Finite Larmor Radius Effects

Let us consider the particle trajectory in the presence of static magnetic field $\mathbf{B}_0(x)$ in z-direction at time t , i.e., $\mathbf{v} \equiv \mathbf{v}(t) = (v_{\perp} \cos \phi, v_{\perp} \sin \phi, v_{\parallel})$, we can write for time $t' = t - \tau$ as $x' \equiv x(t') = x(t) + (v_{\perp}/\Omega)(\sin \phi - \sin(\phi + \Omega\tau))$ and $\mathbf{v}' \equiv \mathbf{v}(t') = (v_{\perp} \cos(\phi + \Omega\tau), v_{\perp} \sin(\phi + \Omega\tau), v_{\parallel})$, where $\Omega = qB_0/m$ is the cyclotron frequency, q and m are the electric charge and mass of the particle, ϕ is the initial gyro phase, and v_{\perp} and v_{\parallel} are components of the electron velocity perpendicular and parallel to the magnetic field, respectively. Considering the electric field perturbation: $\mathbf{E}(\mathbf{r}, t) = \mathbf{E}(x) \exp(i k_{\parallel} z - i \omega t)$, the linearized Vlasov equation leads to the induced current expressed as

$$\begin{aligned} \mathbf{j}(x) &= \int d\mathbf{v} q\mathbf{v} \int_{-\infty}^t d\tau \frac{q}{m} e^{i(\omega - k_{\parallel} v_{\parallel})\tau} \\ &\times [\mathbf{E}(x') + \mathbf{v}' \times \mathbf{B}(x')] \cdot \frac{\partial f_0(x_0, \mathbf{v}')}{\partial \mathbf{v}'}, \end{aligned} \quad (1)$$

where x_0 is the guiding center position. Using the anisotropic Maxwellian distribution function

$$\begin{aligned} f_0(x_0, \mathbf{v}) &= n_0(x_0) \left(\frac{m}{2\pi T_{\perp}(x_0)} \right)^{3/2} \left(\frac{T_{\perp}(x_0)}{T_{\parallel}(x_0)} \right)^{1/2} \\ &\times \exp \left\{ -\frac{mv_{\perp}^2}{2T_{\perp}(x_0)} - \frac{mv_{\parallel}^2}{2T_{\parallel}(x_0)} \right\}, \end{aligned} \quad (2)$$

the induced current density is reduced to

$$\begin{aligned} \mathbf{j}(x) &= \frac{n_0(x_0)q^2}{T_{\perp}(x_0)} \left(\frac{m}{2\pi T_{\perp}(x_0)} \right)^{3/2} \left(\frac{T_{\perp}(x_0)}{T_{\parallel}(x_0)} \right)^{1/2} \\ &\times \int_{-\infty}^{\infty} dv_{\parallel} \int_0^{\infty} dv_{\perp} \int_0^{2\pi} d\phi \int_0^{\infty} d\tau \\ &\times \exp \left\{ -\frac{mv_{\perp}^2}{2T_{\perp}(x_0)} - \frac{mv_{\parallel}^2}{2T_{\parallel}(x_0)} + i(\omega - k_{\parallel} v_{\parallel})\tau \right\} \\ &\times \begin{pmatrix} v_{\perp} \cos \phi \\ v_{\perp} \sin \phi \\ v_{\parallel} \end{pmatrix} (G_x \quad G_y \quad G_z) \cdot \mathbf{E}(x'), \end{aligned} \quad (3)$$

where

$$\begin{aligned} G_x &= \left[1 - \left(1 - \frac{T_{\perp}}{T_{\parallel}} \right) \frac{k_{\parallel} v_{\parallel}}{\omega} \right] v_{\perp}^2 \cos(\phi + \Omega\tau) \\ G_y &= \left[1 - \left(1 - \frac{T_{\perp}}{T_{\parallel}} \right) \frac{k_{\parallel} v_{\parallel}}{\omega} \right] v_{\perp}^2 \sin(\phi + \Omega\tau) \\ G_z &= \frac{T_{\perp}}{T_{\parallel}} v_{\perp}^2 v_{\parallel} - i \left(1 - \frac{T_{\perp}}{T_{\parallel}} \right) \frac{v_{\perp}^2 v_{\parallel}}{\omega} \cos(\phi + \Omega\tau) \frac{\partial}{\partial x'}. \end{aligned}$$

Here, the transformation from the velocity space variables (v_{\perp}, ϕ) to the particle position x' and the guiding center position x_0 is of prime importance. The relation between them is established through the unperturbed orbit, $x = x_0 - (v_{\perp}/\Omega) \sin \phi$ and $x' = x_0 - (v_{\perp}/\Omega) \sin(\phi + \Omega\tau)$. The Jacobian of this transformation is given by $J \equiv -\Omega^2/v_{\perp} \sin \Omega\tau$. The integrand in eq. (3) is a periodic function w.r.t. $\Omega\tau$ which can be expressed as Fourier series and easily integrated over τ . The integration over v_{\parallel} can be expressed by the plasma dispersion function $Z(\eta)$ with $\eta \equiv (\omega - n\Omega)/(\sqrt{2}k_{\parallel}v_{T\parallel})$ where $v_{T\parallel} = (T/m)^{1/2}$. Finally, the expression for induced current becomes

$$\mathbf{j}(x) = \int_{-\infty}^{\infty} dx' \overleftrightarrow{\sigma}(x, x') \cdot \mathbf{E}(x'), \quad (4)$$

and the explicit form of conductivity tensor $\overleftrightarrow{\sigma}(x, x')$ is given in Appendix. The dielectric tensor $\overleftrightarrow{\epsilon}(x', x)$ is the sum of the conductivity tensor of species s and the contribution from the displacement current,

$$\overleftrightarrow{\epsilon}(x', x) = \delta(x - x') + \frac{i}{\omega\epsilon_0} \sum_s \overleftrightarrow{\sigma}(x, x'). \quad (5)$$

Using this dielectric tensor, Maxwell's equation is expressed as

$$\begin{aligned} \nabla \times \nabla \times \mathbf{E}(x) &= \frac{\omega^2}{c^2} \int_{-\infty}^{\infty} dx' \overleftrightarrow{\epsilon}(x, x') \cdot \mathbf{E}(x') \\ &= i\omega\mu_0 \mathbf{j}_{\text{ext}}(x). \end{aligned} \quad (6)$$

3. 1D Kinetic Full Wave Analysis of O-X-B Mode Conversion

We have solved eq. (6) in a slab model numerically by using the finite element method and analyzed the mode conversion and power absorption. The plasma parameters

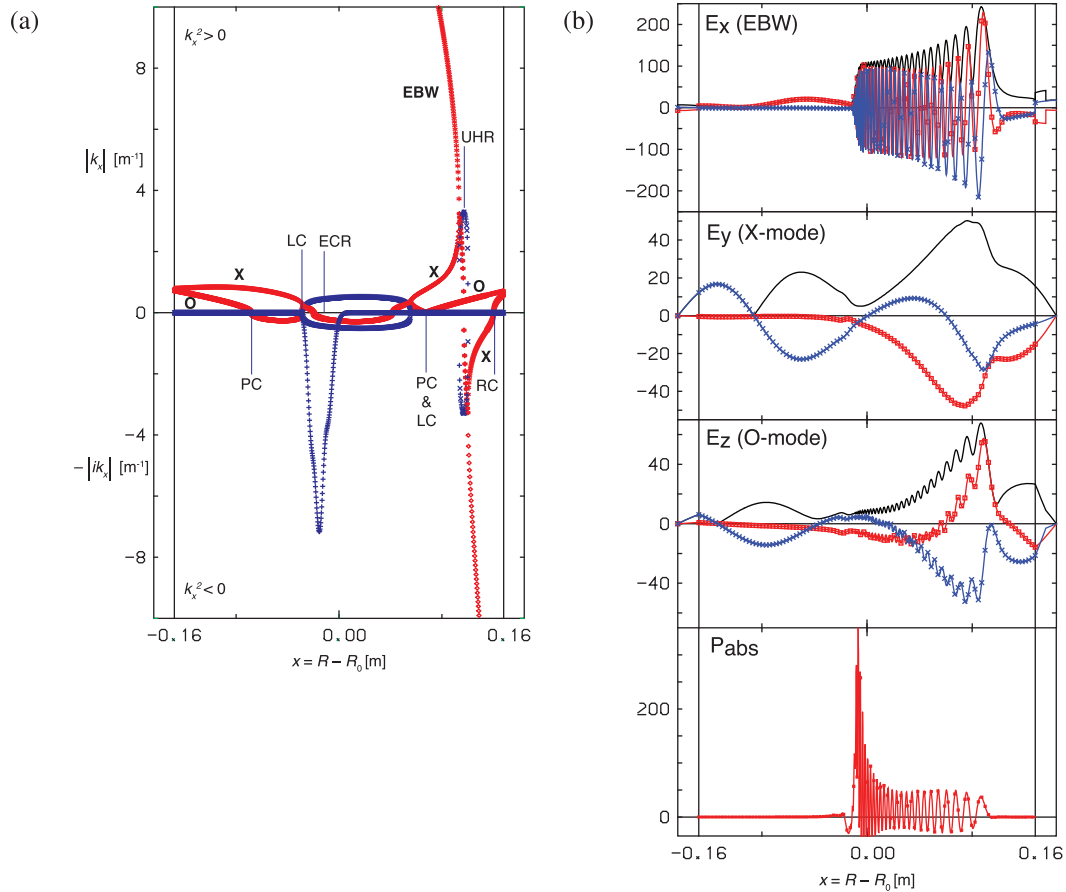


Fig. 1 (a) Wave number k_x as a function of major radius $x = R - R_0$ obtained from the dispersion relation. The red and blue marks indicate the real and imaginary parts of the wave number, respectively. The marks in the upper half plane corresponds to propagating waves, $k_x^2 > 0$, and the lower half plane evanescent waves, $k_x^2 < 0$. (b) Profiles of the wave electric field and the power deposition along x major radius for $T(0) = 500$ eV, $k_z = 32$ m $^{-1}$. The red line indicates the real part of the wave electric field, the blue line the imaginary part, and the black line the absolute value, respectively.

of the small-size spherical tokamak (LATE) are considered. Major radius of the device $R_0 = 0.22$ m, minor radius $a = 0.16$ m, central magnetic field is $B_0 = 0.08$ T, central electron density is 10^{17} m $^{-3}$ and the frequency of the wave excited by antenna current is 2.45 GHz. The temperature profile is parabolic and the density profile is the square root of the parabolic. In the following calculation, 1000 mesh points are used.

Figure 1 (a) shows the wave number k_x as a function of major radius $x = R - R_0$ obtained from the dispersion relation for the optimum parallel wave number $k_z = 32$ m $^{-1}$. The vertical axis indicates $|k_x|$ for propagating modes in the upper half plane and $-|ik_x|$ for evanescent modes in the lower half plane. For this value of k_z , both the plasma cutoff (PC: $\omega^2 = \omega_p^2$) of the O-mode and the left-hand-cutoff (LC) of the X-mode are very close to each other around $x = 0.085$ m. The O-mode is mode-converted to the X-mode at PC & LC and the X-mode is mode converted to the EBW near the UHR after changing the direction of propagation (mode conversion from the fast X-mode to the slow X-mode). The EBW propagates inwards with increasing wave number towards the high field side, and is absorbed

at the ECR.

The wave electric field structure and the power deposition profile calculated by the TASK/W1 code for the parameters of Fig. 1 (a) are shown in Fig. 1 (b). For input power of 1 W, the unit of the wave electric field is V/m, and that of absorbed power density is W/m 3 . The wave is excited as an O-mode by the antenna current in the z direction at $R - R_0 = 0.17$ m. The parallel component E_z indicates the sum of the O-mode component and the electrostatic component $-i k_z \Phi$ of the wave. Most of the O-mode is mode-converted to the X-mode component E_y , and the other part penetrates the evanescent layer to the high field side. Though a part of the X-mode returns to the plasma surface $x = 0.16$ m, most of the wave energy is converted to the electrostatic Bernstein mode near the UHR, $x = 0.12$ m. The electrostatic component is dominant in the x component of the wave electric field E_x , since the wavelength of the Bernstein is very short and the wave number k_x is much higher than those of the X- and O-mode. The Bernstein wave propagates towards the high density region and is absorbed near the fundamental ECR around of $x = -0.1$ m. The absorbed power density $p_{abs}(x)$ is simply calculated by

$P_{\text{abs}} = \mathbf{j}^* \cdot \mathbf{E}$ and oscillates owing to the interference between the EBW and the X- mode. This comes from the ambiguity between the kinetic power absorption and the gradient of kinetic power flux. More rigorous definition of P_{abs} is necessary for positive power absorption density.

The injection angle dependence of the mode conversion efficiency is examined by the k_z dependence of the antenna loading resistance. Preliminary results suggest that the antenna loading resistance has a maximum at the optimum angle, $k_z = 32 \text{ m}^{-1}$, and decreases to about 30% for $k_z = 24 \text{ m}^{-1}$ and $k_z = 40 \text{ m}^{-1}$.

4. Summary

We have made kinetic full wave analysis of electron cyclotron waves for O-X-B mode conversion by 1D hot plasma model by employing the TASK/W1 code. Such analysis using the integral form of dielectric tensor derived by following the unperturbed particle orbit successfully describes the O-X-B mode conversion near the UHR layer and absorption near the ECR layer. More systematic analyses of parameter dependence and quantitative comparison with analytical estimates will be reported in a separate paper.

Acknowledgment

This work is supported by Grant-in-Aid for Research Fellows with JSPS KAKENHI Grant Number 26-04380 from JSPS, Japan.

Appendix

The integral form of the conductivity tensor is written as

$$\overleftrightarrow{\sigma}(x, x') = \int_{-\infty}^{\infty} dx_0 \frac{in_0 q^2}{m\omega} \left(\frac{\Omega}{v_{T\perp}} \right)^2 \sum_{n=-\infty}^{\infty} \overleftrightarrow{H}(x, x', x_0), \quad (\text{A.1})$$

where the components of the tensor \overleftrightarrow{H} are given by

$$\begin{aligned} H_{xx} &= -nA_1 F_n^{(2)} \\ H_{yx} &= iA_1(X - Y) \left\{ (X - Y)F_n^{(3)} - (X + Y)F_n^{(4)} \right\} \\ H_{zx} &= -iA_2 \left\{ (X - Y)F_n^{(3)} - (X + Y)F_n^{(4)} \right\} \\ H_{xy} &= -iA_1(X + Y) \left\{ (X + Y)F_n^{(3)} - (X - Y)F_n^{(4)} \right\} \\ H_{yy} &= -A_1(X + Y)(X - Y)F_n^{(1)} \\ H_{zy} &= A_2(X + Y)F_n^{(1)} \\ H_{xz} &= iA_2 \left\{ (X + Y)F_n^{(3)} - (X - Y)F_n^{(4)} \right\} \end{aligned}$$

$$H_{yz} = A_2(X - Y)F_n^{(1)}$$

$$H_{zz} = \frac{\sqrt{2}v_{T\parallel}\eta}{v_{T\perp}} A_2 F_n^{(1)},$$

with

$$X \equiv \frac{\Omega}{v_{T\perp}} \left(x_0 - \frac{x + x'}{2} \right), \quad Y \equiv \frac{\Omega}{2v_{T\perp}}(x - x').$$

The kernel function $F_n^{(i)}$ is defined by

$$F_n^{(i)}(X, Y) \equiv \frac{1}{2\pi^2} \int_0^\pi d\theta \times \exp \left[-\frac{X^2}{1 + \cos \theta} - \frac{Y^2}{1 - \cos \theta} \right] f_n^{(i)}(\theta),$$

with

$$f_n^{(i)}(\theta) = \begin{cases} \frac{\cos n\theta}{\sin \theta} & (i = 1) \\ \sin n\theta & (i = 2) \\ \frac{\sin n\theta}{\sin^2 \theta} & (i = 3) \\ \frac{\cos \theta \sin n\theta}{\sin^2 \theta} & (i = 4). \end{cases}$$

Finally the coefficients A_1 and A_2 are given by

$$\begin{aligned} A_1 &\equiv \frac{\omega}{\sqrt{2}k_{\parallel}v_{T\parallel}} Z(\eta) + \left(1 - \frac{T_{\perp}}{T_{\parallel}} \right) \frac{Z'(\eta)}{2}, \\ A_2 &\equiv \frac{\omega}{2k_{\parallel}v_{T\perp}} \left\{ \frac{T_{\perp}}{T_{\parallel}} + n \frac{\Omega}{\omega} \left(1 - \frac{T_{\perp}}{T_{\parallel}} \right) \right\} Z'(\eta). \end{aligned}$$

- [1] N.J. Fisch, Rev. Mod. Phys. **59**, 175 (1987).
- [2] R. Prater, J. Fusion Energy **9**, 19 (1990).
- [3] R. Prater, Phys. Plasmas **11**, 2349 (2004).
- [4] B. Lloyd, Plasma Phys. Control. Fusion **40**, A119 (1998).
- [5] J. Urban *et al.*, Nucl. Fusion **51**, 083050 (2011).
- [6] J. Preinhaelter and V. Kopecky, J. Plasma Phys. **10**, 1 (1973).
- [7] H.P. Laqua *et al.*, Phys. Rev. Lett. **78**, 3467 (1997).
- [8] H.P. Laqua, Plasma Phys. Control. Fusion **49**, R1 (2007).
- [9] S. Shiraiwa *et al.*, Phys. Rev. Lett. **96**, 185003 (2006).
- [10] H. Idei *et al.*, J. Plasma Fusion Res. SERIES **8**, 1104 (2009).
- [11] H. Igami *et al.*, Nucl. Fusion **49**, 115005 (2009).
- [12] T. Maekawa *et al.*, J. Phy. Soc. Jpn. **48**, 247 (1980).
- [13] A. Fukuyama, Fusion Eng. Des. **53**, 71 (2001).
- [14] M. Brambilla, Plasma Phys. Control. Fusion **41**, 1 (1999).
- [15] E.F. Jaeger *et al.*, Phys. Plasmas **9**, 1873 (2002).
- [16] O. Sauter and J. Vaclavik, Nucl. Fusion **32**, 8 (1992).
- [17] A. Fukuyama *et al.*, Proc. 21st Fusion Energy Conf., Chengdu, China, 2006, TH0P6-10, IAEA (2006).